euronoise 2021
25th to 27th of October
Madeira, Portugal - online

FDTD Simulation Study of Acoustic Enclosure Shape

Zackery Belanger[1], Elizabeth Teret[1]

[1]Arcgeometer LC
zb@arcgeometer.com
et@arcgeometer.com

Abstract
In acoustics, parametric design often means optimization. In this paper, FDTD simulations are evolved in 2D, reflective enclosures of equal area and varying shape, while the sound distribution is monitored using the Kolmogorov-Smirnov statistical test. The shapes studied are varied geometrically, in an attempt to understand the geometric properties of enclosures that determine the evolution of sound propagating within. Results indicate that enclosures may exhibit three regions of behavior, corresponding to enclosures with flat sides, concave interiors, and convex interiors. Early-stage architectural design decisions may benefit from these results.

Keywords: enclosure, FDTD, shape, concave, convex

1 Introduction

This work aims to inform the architectural design process by gleaning insight into the relationship between enclosure shape and the evolution of sound fields within. Sound is spatial and temporal, and the real and virtual microphones used to study sound are spatially-limited. A diffuse field is usually assumed, so that what is learned at a handful of locations generally applies to the room as a whole. An example is the identification of a transition time, or mixing time, in an impulse response, beyond which the reflections can be treated stochastically to save computing power [1] [2] [3]. However, microphones can obscure the initial spatial development of a sound field, especially in spaces that prevent the development of diffuse fields.

In this work, finite-difference time domain (FDTD) simulations are used to study wave behavior in the time domain. Room boundaries are treated as fully reflective, without absorption of any kind, since the behavior of enclosure shape is the topic of interest. We intentionally do not attempt to reproduce realistic rooms, in order to study the lossless effect of enclosure geometry. This work also recognizes the validity of parametric approaches that differ from CAD sliders and optimization, as exemplified by equations such as Sabine's for reverberation time, in which parameters such as room volume predict aspects of the acoustics of rooms. Our goal is to use incrementally-shaped enclosures to gain insight into the process of room shapes dissipating sound energy. The simulations produced are also excellent, easily readable, visual illustrations of the acoustic character of spaces that alone could be used as training tools for architects.

As with all models and processes, those utilized here have limitations. Any conclusions drawn from the FDTD method employed are limited by the accuracy of FDTD itself. The computational cost limits this study to 2D, though general results are expected to extend to 3D. Ultimately, we hope this methodology encourages architects and designers to begin with room shapes that are acoustically advantageous, rather than unknowingly beginning with a shape that will require correction. This work aims for the initial moments of the design process, as the architect, often without an expert in acoustics, first puts pencil to paper and sets a geometric direction that will be difficult and expensive to undo.

Much related work has been accomplished by others. The sphere, as an idealized and predictable enclosure, has allowed exploration of less predictable properties, as Joyce did in a study of surface roughness [4]. Some spaces develop stable reflection patterns that prevent ergodicity or mixing, and "non-ergodic rooms exhibit varying reverberation" [1]. The separation between room geometry and wall admittance was described by Bilbao and Hamilton [5] as a part of their effort to stabilize FDTD simulations. Those who look for mixing times in impulse responses often use statistical analyses, with the premise that "the diffuse sound field is assumed to be a Gaussian process"[6]. According to Mikio Tohyama, the histogram of an even energy distribution is equal to an exponential distribution [7]. FDTD has been used in the field of acoustics since at least 1994, when the method was described by Bottledooren [8], and adding frequency dependent boundary conditions increases the complexity of simulation [9]. Over time, advances in this field of inquiry have increased our ability to include and decipher ever more detailed information from FDTD simulations [10][11]. The study of idealized enclosures with reflective walls and simple geometry finds precedent in earlier acoustic studies, such as Bolt et al [12], conducted before computer processing made more realistic acoustic simulations possible. The hypothesis that enclosure shape will determine mixing time is rooted in billiard theory, and the chaotic behavior of acoustic rays in irregularly shaped enclosures [13][14]. The methods used in this research were originally implemented in thesis work by Belanger [15], and were evolved for the work presented here.

2 Methods

2.1 FDTD simulation method

The 2D shapes to be studied were generated in Rhinoceros modeling software. They were discretized using a custom Grasshopper script, in Rhino, that overlays a variable-resolution grid of lines onto the shape, and records the coordinates of intersection points between the two systems. Those points are then exported and read into a custom Python FDTD simulation script. This system allows for any arbitrarily shaped geometries.

The simulation script uses a non-staggered 3D compact explicit scheme on a rectilinear grid - a specific variant known as interpolated wideband [16]. The 3D wave equation for sound propagation in air is:

$$\frac{\partial^2 p}{\partial t^2} = c^2 \left(\frac{\partial^2 p}{\partial x^2} + \frac{\partial^2 p}{\partial y^2} + \frac{\partial^2 p}{\partial z^2} \right) \tag{1}$$

where p is pressure and c is the speed of sound. Compact explicit schemes can approximate this equation as:

$$\partial_t^2 p_{l,m,i}^n = \lambda^2 \left[\left(\partial_x^2 + \partial_y^2 + \partial_z^2 \right) + a \left(\partial_x^2 \partial_y^2 + \partial_y^2 \partial_z^2 + \partial_x^2 \partial_z^2 \right) + b \partial_x^2 \partial_y^2 \partial_z^2 \right] p_{l,m,i}^n \tag{2}$$

where p is the updated pressure, n is the time step index, a and b are free numerical parameters, and l, m and i are the spatial indexes. λ is the Courant number, and is defined as

$$\lambda = c * \frac{\partial t}{\partial x} \tag{3}$$

which determines the timestep given the spatial resolution and Courant value, which is 1/√2 for the 2D simulations in this work. The second-order derivative centered finite-difference operators are defined as follows:

$$\begin{aligned} \partial_t^2 p_{l,m,i}^n &\equiv p_{l,m,i}^{n+1} - 2p_{l,m,i}^n + p_{l,m,i}^{n-1} \\ \partial_x^2 p_{l,m,i}^n &\equiv p_{l+1,m,i}^n - 2p_{l,m,i}^n + p_{l-1,m,i}^n \\ \partial_y^2 p_{l,m,i}^n &\equiv p_{l+1,m,i}^n - 2p_{l,m,i}^n + p_{l,m-1,i}^n \end{aligned} \tag{4}$$

$$\partial_z^2 p_{l,m,i}^n \equiv p_{l,m,i+1}^n - 2p_{l,m,i}^n + p_{l,m,i-1}^n$$
$$p_{l,m,i}^n \equiv p(x,y,z,t)|_{x=lX,y=mX,t=nT}$$

These operators can be applied to equation 2 to obtain the update equation for general compact schemes:

$$\begin{aligned} p_{l,m,i}^n = {} & d_1\left(p_{l+1,m,i}^n + p_{l-1,m,i}^n + p_{l,m+1,i}^n + p_{l,m-1,i}^n + p_{l,m,i+1}^n + p_{l,m,i-1}^n\right) \\ & + d_2\left(p_{l+1,m+1,i}^n + p_{l+1,m-1,i}^n + p_{l+1,m,i+1}^n + p_{l+1,m,i-1}^n + p_{l,m+1,i+1}^n\right. \\ & + p_{l,m+1,i-1}^n + p_{l,m-1,i+1}^n + p_{l,m-1,i-1}^n + p_{l-1,m+1,i}^n + p_{l-1,m-1,i}^n \\ & \left. + p_{l-1,m,i+1}^n + p_{l-1,m,i-1}^n\right) \\ & + d_3\left(p_{l+1,m+1,i+1}^n + p_{l+1,m-1,i+1}^n + p_{l+1,m+1,i-1}^n + p_{l+1,m-1,i-1}^n\right. \\ & \left. + p_{l-1,m+1,i+1}^n + p_{l-1,m-1,i+1}^n + p_{l-1,m+1,i-1}^n + p_{l-1,m-1,i-1}^n\right) \\ & + d_4\left(p_{l,m,i}^n - p_{l,m,i}^{n-1}\right) \end{aligned} \tag{5}$$

where the interpolated wideband variant requires $d_1 = 1/4$, $d_2 = 1/8$, $d_3 = 1/16$, and $d_4 = -3/2$. While conformal methods exist that allow the use of curved boundaries, a stepped method with high spatial resolution was chosen, the computing power for which remains reasonable in 2D. The resolution used for all geometries is 1 centimeter, or 100 points per meter, which is adequate given the relative simplicity of all forms and limited frequencies studied.

This simulation method uses pressure-release boundaries, where the pressure at points defining the enclosure geometry are set to zero and therefore represent a completely reflective condition. This allows the study of geometric influence, without material flex or locally absorptive surfaces. It can be assumed that any real condition would be marked by increased absorption and would yield a quicker dissipation of acoustic energy.

2.2 Excitation pulse

The spatial resolution determines the temporal resolution, or sampling frequency, of the simulation. With a fixed sound speed of 340.3 meters/second and 100 sample points per meter, the sampling frequency is 34,030 Hz. In all FDTD simulations, there is dispersion error, particularly in axial directions and at high frequencies. This is reduced by the selection of a Courant number of $1/\sqrt{2}$ (for 2D), and by the frequency limits of the excitation pulse. The FDTD results are considered accurate only for frequencies up to 1/10 of the sampling frequency [17]. In this case, the simulation should produce reliable results up to 3,403 Hz.

The sound source for the simulations is a Gaussian pulse:

$$p = e^{a\left(x^2+y^2\right)} \tag{6}$$

where the pulse number a determines the frequency content of the excitation pulse. The pulse is inserted into the simulation at the zeroth time step. However, it can be evaluated in the time domain, as each physical distance from the center can be converted into a time difference. We have determined that a pulse number of -256 creates a frequency range that lies mostly below the 3,403 Hz cutoff, limiting the information to those frequencies that show very little dispersion error. A Fourier transform converts this time-domain pulse into the frequency domain for graphing.

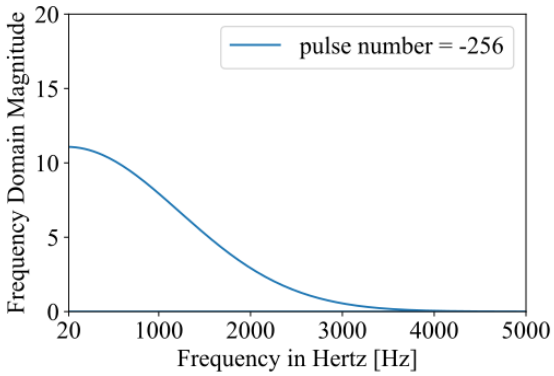

Figure 1: The frequency spectrum of the pulse used as a sound source for simulations

2.3 Statistical analysis

To analyze only the energy within the enclosure, the script sets all pressure values to zero, then initializes a preliminary FDTD simulation. As this simulation progresses, the number of points with pressure equal to zero is monitored as it decreases, as interior points are jostled. When the number of points equal to zero stabilizes, it means the wavefront has reached every point within the enclosure. All points with pressure levels other than zero are then marked as interior, the simulation is reset, and the main simulation is begun.

The simulation calculates sound pressure levels at every point in the enclosed space, which are squared to represent sound energy. A histogram is then created of these energy levels and compared to an exponential distribution at every timestep using the Kolmogorov-Smirnov (K-S) test, which is a non-parametric comparison of two probability distributions. A value of 1 indicates an energy distribution that is not at all exponential, and a value of 0 is a perfect exponential distribution. By calculating the K-S statistic at each timestep and monitoring its evolution, the approach to a mixing condition can be characterized. This definition of mixing as statistically equal energy distribution in a room is different from a diffuse sound field in that mixing is an idealized concept that does not consider absorption, either in severity or distribution [18].

3 Results

Room shapes studied are grouped into five series, which are listed in Table 1. Internal area is held constant at 78.54 square meters - the area of a circle of diameter 10 meters. In each series, an aspect of enclosure shape is parametrically altered, such as curving the boundary. All simulations were run for 500 milliseconds.

Table 1 – Enclosure Shapes and Properties

shape type	number tested	property varied	internal area
circle	1	n/a	78.54 m^2
rectangles	10	proportion	78.54 m^2
regular polygons	11	number of sides	78.54 m^2
curved squares	51	angle of vertices / curve of sides	78.54 m^2
curved triangles	43	angle of vertices / curve of sides	78.54 m^2

3.1 The circle

Our exploration begins with a circle. In a reflective circle with a centralized, point sound source, sound will never dissipate. The circular sound wave will expand to the borders, reflect, then contract to the center,

repeatedly. In 3D, a spherical enclosure and central spherical source would behave in the same way. A plot of the K-S test results reveals the expected repeated behavior of reflection at the boundary and concentration at the center.

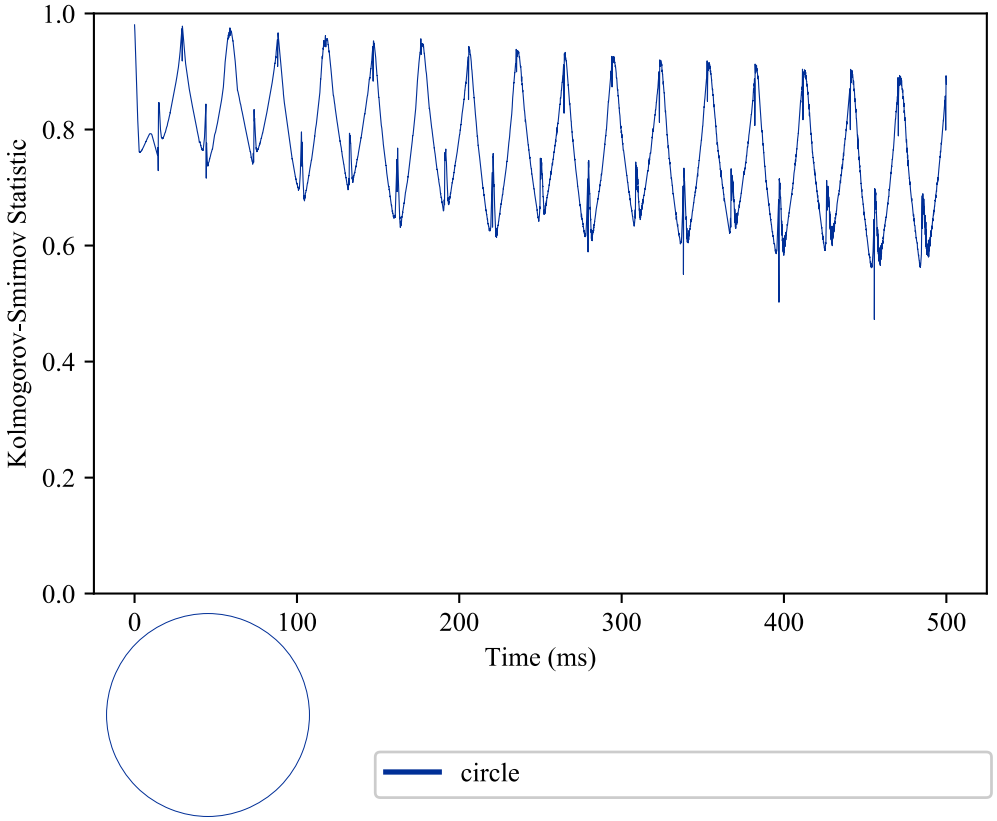

Figure 2 - Energy distribution over time in a circular enclosure

The simulation begins with an impulse in the center of the circle, and shows a K-S value of nearly one, corresponding to a high concentration of energy. As the wave expands outward and the sound distribution increases, the K-S value is reduced. When the wave encounters the enclosure, it reverses direction and increases in concentration as it travels back toward the center of the circle. The regular increase and decrease of K-S values in the plot corresponds to the inward and outward movement of the wavefront. The frequency of this oscillation is determined by the speed of sound and the size of the enclosure. Also notable is the wavefield degradation, or walking of the curve, over time; this is an artifact of the dispersion error discussed in the Methods section above. This example, where the enclosure has a minimal perimeter, and is normal to the direction of propagation, serves as a baseline for other shapes.

3.2 Rectangles

Many physical rooms are rectangular in plan, so a series of rectangles is relevant to the design process. The first enclosure in the series is a square with an area of 78.54 square meters, matching the circle in the first study. Subsequent rectangles maintain area but increase in ratio of length to width. The increment of change between rectangles is constant, and is measured in circle defect, which is the ratio of perimeter to the circumference of a circle of equal area. A series of 10 rectangles was studied, with the final rectangle in the series exhibiting a circle defect equal to that of an equilateral triangle.

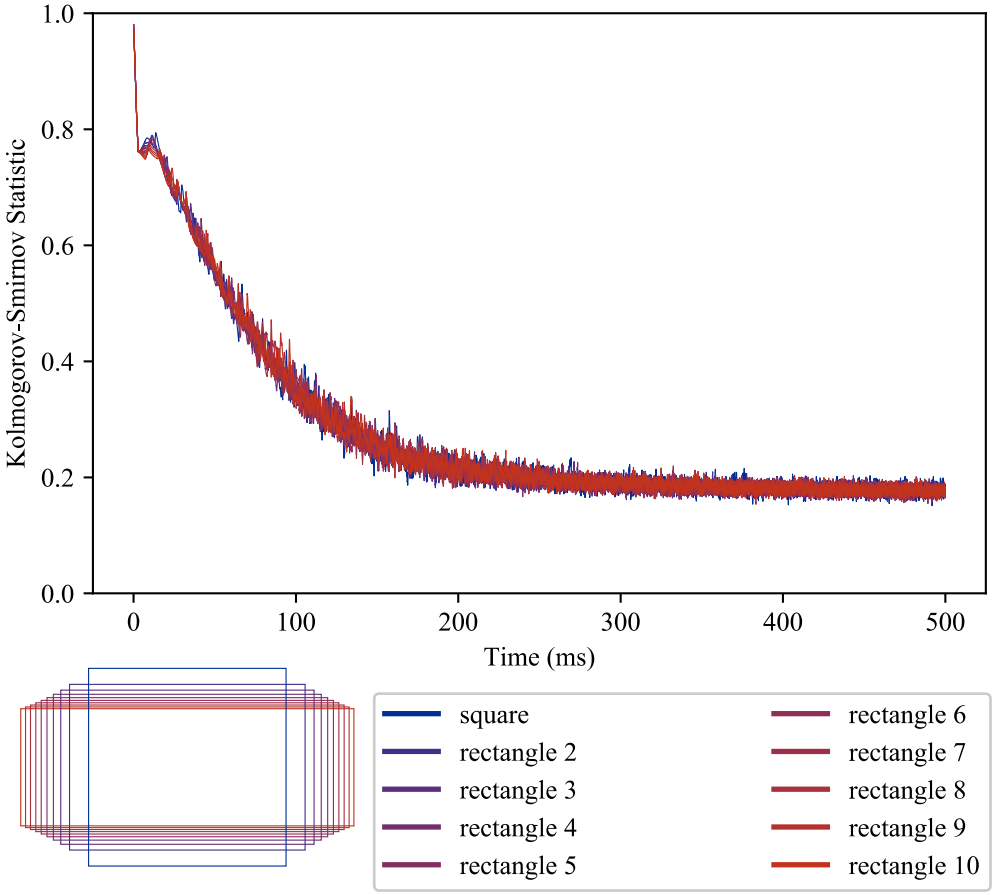

Figure 3 – Energy distribution over time in 10 rectangular enclosures

The results show that the changes in length/width ratio made little difference in the rate of sound distribution for rectangles. The K-S value curve shapes are nearly identical for all 10 rectangles studied.

3.3 Regular polygons

This series is a progression toward the idealized circular condition, inspired by the idea in calculus that a circle can be approximated by regular polygons of increasing number of sides. The triangle is the coarsest approximation, and the number of sides is increased until a dodecagon is reached. For reference, the previous results of the circle have also been included.

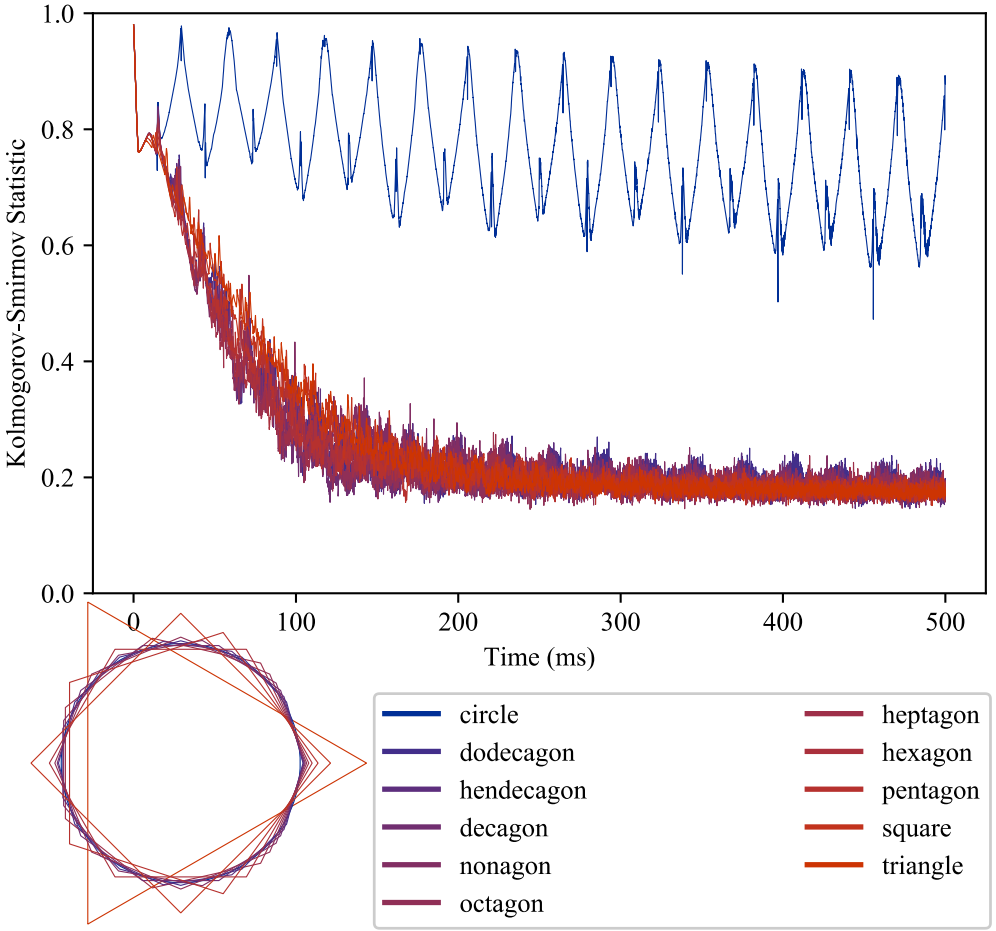

Figure 4 – Energy distribution over time in a circle and 10 regular polygons

The plot of the K-S values over time shows considerable mixing for all shapes in comparison with the circle, along with some degree of oscillation, though significantly reduced in comparison with the circle. The behavior is similar for all regular polygons, as all K-S curves have similar shape and lie roughly on each other, though not as tightly as for the rectangular series. This may be unexpected, as the polygons with more sides are more similar to the circle and could have been expected to mix significantly slower than the few-sided polygons. In fact, the triangle can be seen to have the slowest mixing of all.

3.4 Curved squares

As with the regular polygons, this series is conceived as an incremental departure from the circular enclosure. Each ‘square’ has four curved sides. If one were to divide a circle into four equal semicircles and add a vertex at the boundary between each semicircle, that would be the condition labeled a 180 degree vertices, since each vertex has two curves that meet at a 180 degree angle. Using this condition as a starting point, the angle at those vertices was incrementally changed, allowing the connecting curves to flex appropriately, to produce shapes with concave and convex sides, and a square (90 degree vertices). The expectation would be that, as the vertex angles decrease, and the shapes would become less circular, the sound energy would distribute faster.

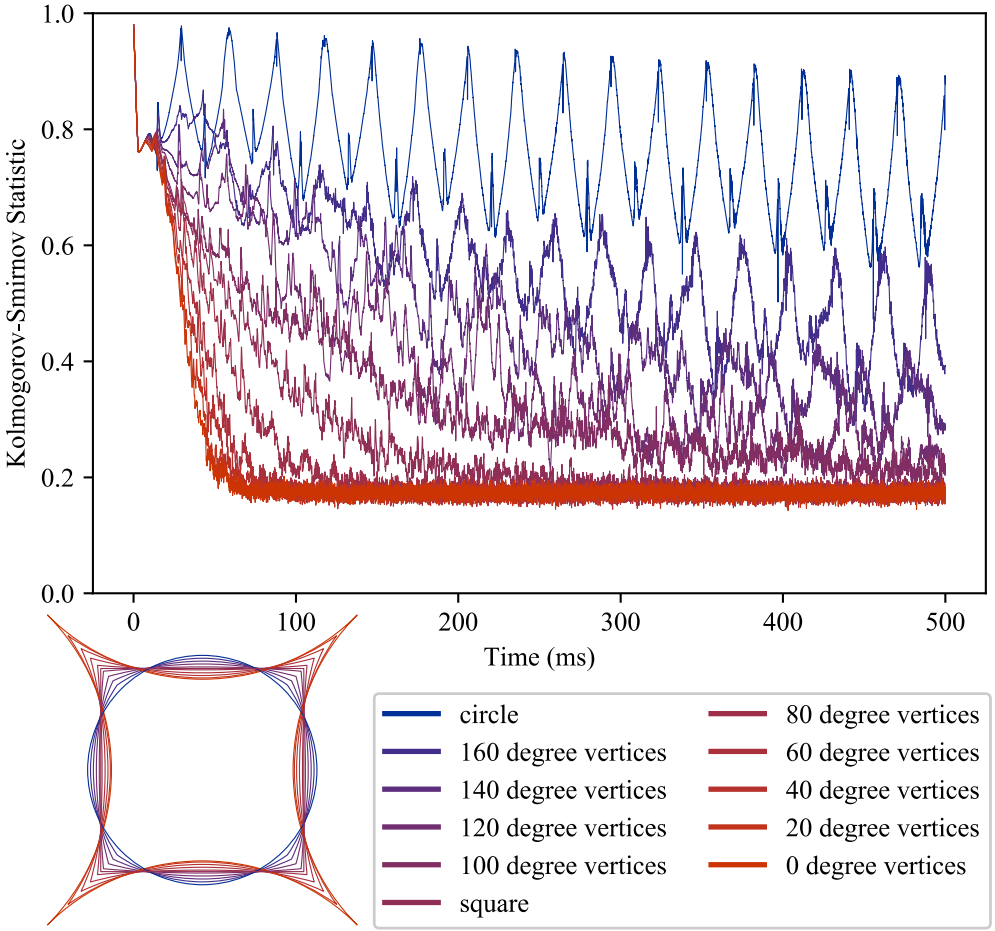

Figure 5 – Energy distribution over time in four sided figures with curved sides

This plot of K-S values shows that this series yields no surprises, with a higher rate of sound distribution as the shapes diverged from the circle. The plot shows 11 conditions in 20 degree increments, but simulations were conducted at up to 2 degree increments, for 51 total conditions. The pattern seen in this plot, where K-S values drop more quickly when the vertices are more acute, appears to be consistent and predictable throughout the series.

3.5 Curved triangles

The curved triangles are similar to the curved squares, with vertices that range from 0 degrees to the 180 degree circle.

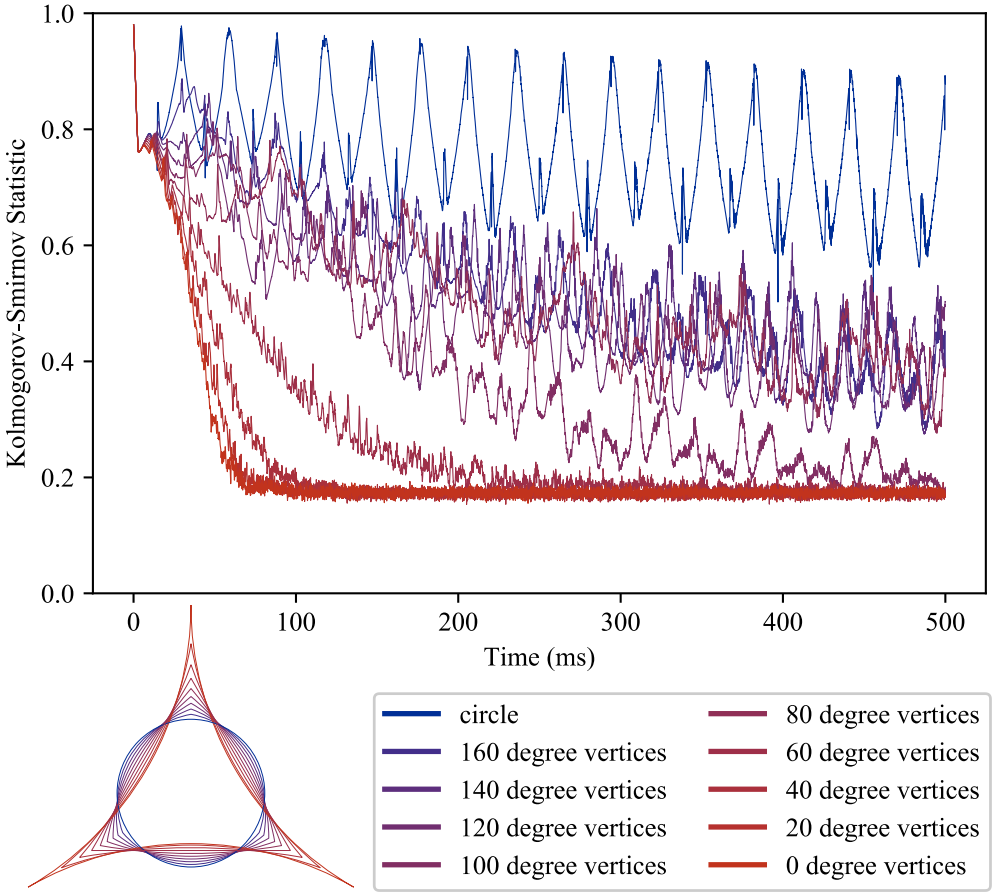

Figure 6 – Energy distribution over time in three sided figures with curved sides

As seen with the curved squares, these 3-sided figures behave in a predictable manner, with the curvature of the sides determining the rate of energy distribution inside the enclosure. 43 total conditions were tested, though the plot is limited to 10 conditions for clarity.

4 Conclusions

In this work, we have described a method for assessing the distribution of simulated sound energy in 2D spaces, and demonstrated, through parametrically varying room shapes, a potential relationship between enclosure shape and the rate of distribution of sound within. Three apparent realms of acoustic behavior were studied: simple convex polygons, curved enclosures with concave interiors, and curved enclosures with convex interiors. While the potentially detrimental influence of concave surfaces - the domes and cylinders of classic architecture - has been understood in architectural acoustics for a long time, this work places such surfaces in the context of enclosure form as a whole, and in relationship to flat and convex forms. The curved enclosures with concave interiors tend to impede the dissipation of sound, while those with convex interiors tend to promote dissipation. Simple convex polygons, with flat sides, appear to be a benchmark which sits between these other two realms, and which all seem to dissipate sound in a similar manner. We submit that this work provides an intuitive basis for the choice of some room shapes at the very beginning of the design process, that goes beyond the limited advice to "avoid focusing shapes" by providing a framework that includes the whole enclosure and the range of enclosure types.

Acknowledgements

This research was funded by Arcgeometer LC. Some concepts were developed during a Research Residency of the first author at the Experimental Media and Performing Arts Center (EMPAC) at Rennselaer.

References

[1] Billon, A.; Embrechts, J.-J. Numerical evidence of mixing in rooms using the free path temporal distribution. *J. Acoust. Soc. Am.*, Vol 130 (3), 2011, pp. 1381–1389.

[2] Defrance, G.; L. Daudet, L.; Polack, J.D. Using Matching Pursuit for estimating mixing time within room impulse responses. *Acta Acust. united with Acust.*, Vol 95 (6), 2009, pp. 1071–1081.

[3] Jeong, C.-H.; Brunskog, J.; and Jacobsen, F. Room acoustic transition time based on reflection overlap. *J. Acoust. Soc. Am.*, Vol 127 (5), 2010, pp. 2733–2736.

[4] Joyce, W.B. Exact effect of surface roughness on the reverberation time of a uniformly absorbing spherical enclosure. *J. Acoust. Soc. Am.*, Vol 64 (5), 1978, pp. 1429–1436.

[5] Bilbao, S.; Hamilton, B. Passive volumetric time domain simulation for room acoustics applications. *J. Acoust. Soc. Am.*, Vol 145 (4), 2019, pp. 2613–2624.

[6] Defrance, G.; Polack, J.D. Measuring the mixing time in auditoria. *Proc. - Eur. Conf. Noise Control*, 2008, pp. 3871–3876.

[7] Tohyama, M. *Sound and Signals*, Springer, Berlin, Germany, 1st Edition, 2013.

[8] Botteldooren, D. Acoustical finite-difference time-domain simulation in a quasi-Cartesian grid. *J. Acoust. Soc. Am.*, Vol 95 (5), 1994, pp. 2313–2319.

[9] Botteldooren, D. Finite-difference time-domain simulation of low-frequency room acoustic problems. *J. Acoust. Soc. Am.*, Vol 98 (6), 1995, pp. 3302–3308.

[10] Vorländer, M. Computer simulations in room acoustics: Concepts and uncertainties. *J. Acoust. Soc. Am.*, Vol 133 (3), 2013, pp. 1203–1213.

[11] Saarelma, J.; Savioja, L. Spatial analysis of modal time evolution in room acoustics. *J. Acoust. Soc. Am.*, Vol 145 (1), 2019, pp. EL116–EL121.

[12] Bolt, R.H.; Doak, P. E.; Westervelt, P. J. Pulse Statistics Analysis of Room Acoustics. *J. Acoust. Soc. Am.*, Vol 22 (3), 1950, pp. 328–340.

[13] Kawabe, T.; Aono, K.; Shin-ya, M. Acoustic ray chaos and billiard system in Hamiltonian formalism (L). *J. Acoust. Soc. Am.*, Vol 113 (2), 2003, pp. 701–704.

[14] Koyanagi, S.; Nakano, T.; Kawabe, T. Application of Hamiltonian of ray motion to room acoustics. *J. Acoust. Soc. Am.*, Vol 124 (2), 2008, pp. 719–722.

[15] Belanger, Z. Sound energy evolution in two-dimensional enclosures as determined with a finite difference time domain method. Rensselaer Polytechnic Institute, 2012.

[16] Kowalczyk, K.; Van Walstijn, M. Room acoustics simulation using 3-D compact explicit FDTD schemes. *IEEE Trans. Audio, Speech Lang. Process.*, Vol 19 (1), 2011, pp. 34–46.

[17] Kowalczyk, K. Boundary and medium modelling using compact finite difference schemes in simulations of room acoustics for audio and architectural design applications. *Electr. Eng.* November, 2008.

[18] Jeong, C. H. Diffuse sound field: Challenges and misconceptions. *INTER-NOISE 2016 - 45th Int. Congr. Expo. Noise Control Eng.*, Hamburg, Germany, August 21-25, pp. 1015–1021.